

PRIMARY RESEARCH ARTICLE

Changes in timing of seasonal peak photosynthetic activity in northern ecosystems

Taejin Park¹  | Chi Chen¹ | Marc Macias-Fauria²  | Hans Tømmervik³  |
 Sungho Choi⁴ | Alexander Winkler^{5,6} | Uma S. Bhatt⁷ | Donald A. Walker⁸ |
 Shilong Piao⁹  | Victor Brovkin⁵ | Ramakrishna R. Nemani¹⁰ | Ranga B. Myneni¹

¹Department of Earth and Environment, Boston University, Boston, Massachusetts

²School of Geography and the Environment, University of Oxford, Oxford, United Kingdom

³Norwegian Institute for Nature Research, FRAM – High North Research Centre for Climate and the Environment, Tromsø, Norway

⁴Rhombus Power Inc., NASA Ames Research Park, Moffett Field, California

⁵Max-Planck-Institute for Meteorology, Hamburg, Germany

⁶International Max-Planck Research School for Earth System Modeling, Hamburg, Germany

⁷Geophysical Institute, University of Alaska Fairbanks, Fairbanks, Alaska

⁸Institute of Arctic Biology, University of Alaska, Fairbanks, Alaska

⁹College of Urban and Environmental Sciences, Peking University, Beijing, China

¹⁰NASA Ames Research Center, Moffett Field, California

Correspondence

Taejin Park, Department of Earth and Environment, Boston University, Boston, MA 02215, USA.
 Email: parktj@bu.edu

Funding information

National Aeronautics and Space Administration, Grant/Award Number: NNX14AI71G, NNX14AP80A and NNX16AO34H; Norges Forskningsråd, Grant/Award Number: 287402 and 270992; Natural Environment Research Council, Grant/Award Number: NE/L011859/1

Abstract

Seasonality in photosynthetic activity is a critical component of seasonal carbon, water, and energy cycles in the Earth system. This characteristic is a consequence of plant's adaptive evolutionary processes to a given set of environmental conditions. Changing climate in northern lands (>30°N) alters the state of climatic constraints on plant growth, and therefore, changes in the seasonality and carbon accumulation are anticipated. However, how photosynthetic seasonality evolved to its current state, and what role climatic constraints and their variability played in this process and ultimately in carbon cycle is still poorly understood due to its complexity. Here, we take the “laws of minimum” as a basis and introduce a new framework where the timing (day of year) of peak photosynthetic activity ($DOY_{P_{max}}$) acts as a proxy for plant's adaptive state to climatic constraints on its growth. Our analyses confirm that spatial variations in $DOY_{P_{max}}$ reflect spatial gradients in climatic constraints as well as seasonal maximum and total productivity. We find a widespread warming-induced advance in $DOY_{P_{max}}$ (-1.66 ± 0.30 days/decade, $p < 0.001$) across northern lands, indicating a spatiotemporal dynamism of climatic constraints to plant growth. We show that the observed changes in $DOY_{P_{max}}$ are associated with an increase in total gross primary productivity through enhanced carbon assimilation early in the growing season, which leads to an earlier phase shift in land-atmosphere carbon fluxes and an increase in their amplitude. Such changes are expected to continue in the future based on our analysis of earth system model projections. Our study provides a simplified, yet realistic framework based on first principles for the complex mechanisms by which various climatic factors constrain plant growth in northern ecosystems.

KEYWORDS

carbon cycle, climate change, climate constraint, earth system model, eddy covariance, gross primary productivity, law of minimum, photosynthetic seasonality, remote sensing

1 | INTRODUCTION

Warming is generally thought to ease climate constraint on photosynthetic activity of vegetation in northern lands. Indeed, recent growing season studies based on ground observation (Parmesan & Yohe, 2003), eddy covariance (Keenan et al., 2014; Richardson et al., 2010), remote sensing (Park et al., 2016; Xu et al., 2013), and model simulation (Duveneck & Thompson, 2017) have concordantly indicated that the growing season duration for northern terrestrial vegetation has significantly extended over the past decades due to both an earlier start and delayed termination. This prolonged growing season over northern land drives a longer carbon assimilation period due to the relaxation of low temperature limits on metabolism, and in turn, increased productivity and carbon uptake have been observed (Forkel et al., 2016; Xu et al., 2013). However, longer and warmer growing seasons also promote environmental conditions that favor surface drying, and thus intensified summer droughts, tree mortality, and wildfires have resulted in summer productivity decline (Barichivich et al., 2014; D'Orangeville et al., 2018; Peng et al., 2011). These consequential dynamics are highly variable in space and over time, and indicate a complex interaction of multiple climate constraints on plant growth and its dynamism (Garonna et al., 2018; Nemani et al., 2003; Reich et al., 2018). To accurately project the response of northern vegetation to future climate, we need to better understand how climate-vegetation interaction has evolved to its current state, and what role climatic constraints and their variability played in this process.

Photosynthetic seasonality is an integrated outcome of how plants adapt to seasonal variations in climatic constraints (Chuine & Beaubien, 2001; Eagleson, 2005; Garonna et al., 2018; Jolly, Nemani, & Running, 2005), and is thus a critical indicator of vegetation-climate interaction. For instance, gross primary productivity (GPP) tracks the seasonal course of temperature in northern high-latitude ecosystems, while the synchrony between GPP and temperature is gradually lost southwards toward warmer and drier environments (see Figure 1 in Rotenberg & Yakir, 2010). The laws of minimum (Blackman, 1905; Liebig, 1841; Sprengel, 1828) explain these shifts in GPP with respect to varying climatic conditions (Eagleson, 2005). The laws state that although photosynthetic activity is controlled by multiple factors (e.g., radiation, temperature, water availability, etc.), the prevailing rate is set by the most deficient of these factors (Blackman, 1905; Liebig, 1841; Sprengel, 1828). This suggests that the timing (day of year) of peak photosynthetic rate ($DOY_{P_{max}}$) during the seasonal course corresponds to the period when the primary climatic factor controlling plant growth is least limiting. This simple yet intuitive indicator has an indispensable role not only indicating the timing and magnitude of resource availability (i.e., constraint) but also the capacity of terrestrial ecosystem productivity (Xia et al., 2015; Zhou et al., 2017). Ongoing climate change in the north is expected to alter the state of climatic constraints on plant growth, and therefore, changes in $DOY_{P_{max}}$ and productivity. Previous studies have observed trends toward an earlier peak of the growing season (Buitenwerf, Rose, & Higgins, 2015; Gonsamo, Chen, & Ooi, 2018). However, the

underlying mechanisms for spatially varying relations between its changes and implications on seasonal total productivity and carbon cycle are still largely unknown.

In this study, we take the "laws of minimum" as a basis and introduce a new framework where the timing of peak photosynthetic activity ($DOY_{P_{max}}$) acts as a proxy for plant's adaptive state to climatic constraints on its growth. Two basic principles formulate this new framework (Figure 1). First, under nonlimiting climatic conditions, $DOY_{P_{max}}$ will show a tendency to coincide with the period of seasonal peak radiation load so as to result in maximum photosynthetic capacity conditions (Bauerle et al., 2012; Eagleson, 2005; Case 1 in Figure 1). Second, if a climatic factor acts as the primary constraint to photosynthetic activity, $DOY_{P_{max}}$ should shift toward the period in the seasonal course at which that limiting resource is more available (Eagleson, 2005; Rotenberg & Yakir, 2010; Cases 2-4 in Figure 1). In this framework, the timings of peak GPP ($DOY_{P_{max}}$) and three climatic factors including temperature ($DOY_{T_{max}}$), radiation ($DOY_{R_{max}}$), and water availability ($DOY_{W_{max}}$) serve as key proxies for climate resource availability. We only introduce these three abiotic controls of GPP because it is widely known that they interact to primarily impose complex and varying limitations on vegetation activity (Nemani et al., 2003). Due to reduced water losses during the cold season over northern terrestrial ecosystems and thermal inertia, a sequential order of the timings of peak climatic factors ($DOY_{W_{max}} < DOY_{R_{max}} < DOY_{T_{max}}$) simplifies our framework (Figure S1). In other words, this suggests that positioning of $DOY_{P_{max}}$ with respect to $DOY_{R_{max}}$ ($\delta DOY_{P,R} = DOY_{P_{max}} - DOY_{R_{max}}$) can indicate the primary climatic constraint on ecosystems, that is, water ($\delta DOY_{P,R} < 0$) or temperature ($\delta DOY_{P,R} > 0$). $\delta DOY_{P,T}$ defined as $DOY_{P_{max}} - DOY_{T_{max}}$ is additionally introduced to subdivide dominant temperature constrained northern ecosystems.

Our primary objectives of this study are twofold: (a) to examine the proposed framework using independent multiple datasets and understand how northern vegetation seasonality has been characterized; and (b) to investigate changes in $DOY_{P_{max}}$ and its impact on seasonal total productivity and carbon cycle. To accomplish the objectives, we apply the proposed framework to GPP dynamics from the satellite observed vegetation photosynthetic activity to evaluate its validity and changes in $DOY_{P_{max}}$. Two independent sources of vegetation productivity (tower-measured GPP and satellite-driven sun-induced fluorescence [SIF]) are used to further test the framework. We use the atmospheric CO_2 observations at Point Barrow (71.3°N, 156.6°W) and two state-of-the-art CO_2 inversion estimates to investigate the potential impact of shifting $DOY_{P_{max}}$ on terrestrial ecosystem carbon cycle. A set of earth system models (ESMs) is additionally introduced to evaluate the reproducibility of the observed $DOY_{P_{max}}$ changes and their consequences under historical and future climate scenarios.

2 | MATERIALS AND METHODS

2.1 | Study area and bioclimatic zones

Only nonagricultural vegetation over north of 30°N is considered in this study to minimize human-induced influence. Three bioclimatic

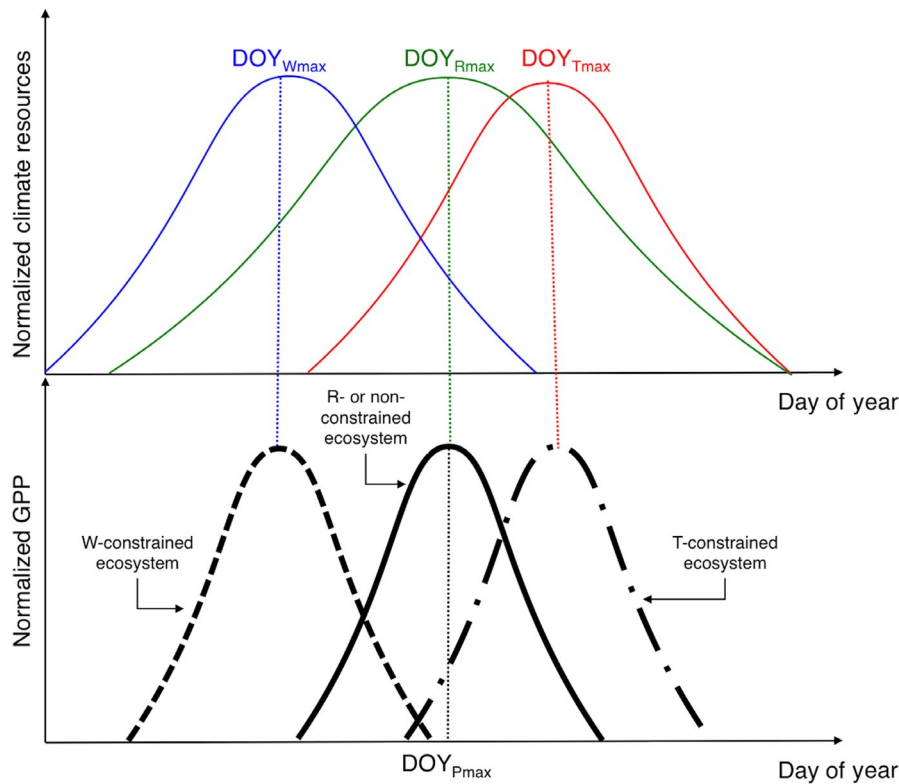


FIGURE 1 Conceptual illustration of the proposed $DOY_{P_{max}}$ framework. Seasonal cycle of temperature (T, red), radiation (R, green), water availability (W, blue), and gross primary productivity (GPP) (P, black) over common northern terrestrial ecosystems. Vertical lines indicate when each variable reaches a maximum state. $DOY_{P_{max}}$, $DOY_{T_{max}}$, $DOY_{R_{max}}$, and $DOY_{W_{max}}$ stand for the day of year when GPP, temperature, radiation, and precipitation reach respective maximum state during each seasonal course of the year. Four idealized cases are shown to demonstrate how photosynthetic seasonality of the ecosystem under given climate constraint differs from each other: non- (solid line, Case 1), temperature- (dot dash line, Case 2), water- (long dash line, Case 3), and radiation- (solid line, Case 4) constrained ecosystems

zones including arctic, boreal, and temperate regions were used to present outcomes of this study. To discriminate the bioclimatic zones, we combined a terrestrial ecoregion scheme (Olson et al., 2001) of the World Wildlife Fund (WWF) and the Moderate Resolution Imaging Spectroradiometer (MODIS) International Geosphere-Biosphere Programme (IGBP) land cover data (Friedl et al., 2010; Collection 5.1). We first used MODIS IGBP to keep only nonagricultural vegetation classes (Class 1–10 and 16). Then, based on the WWF's ecoregion scheme, tundra and boreal forests/taiga ecoregions were assigned into the arctic and boreal bioclimatic zones, respectively. Temperate broadleaf and mixed forests, temperate coniferous forests, temperate grasslands, savannas, and shrublands were identified as the temperate bioclimatic zone. We further excluded the pixels containing more than 25% of cropland based on the International Institute for Applied Systems Analysis cropland fraction data (Fritz et al., 2015).

2.2 | Data and methods

2.2.1 | Multiscale GPP and its proxy: satellite and tower measurements

In this study, we mainly used 17 year (2000–2016) time series of GPP data from the MODIS aboard NASA's Terra satellite (Running, Mu, &

Zhao, 2015) to examine the framework and to investigate $DOY_{P_{max}}$ change in northern lands. The latest version (Collection 6) of MODIS GPP with 8 day temporal composite was spatially aggregated into 0.05 degree grid. Its high temporal frequency is advantageous to capture the seasonal variation of photosynthetic activity. MODIS GPP is based on a production efficiency model that uses the product of the absorbed photosynthetically active radiation by vegetation and a light use efficiency factor. The quality of MODIS GPP datasets has been comprehensively evaluated against multiple eddy-covariance tower measurements of GPP and through intercomparisons with other GPP products (Heinsch et al., 2006; Zhao, Heinsch, Nemani, & Running, 2005).

We additionally introduced satellite-driven SIF and eddy-covariance-based GPP data to verify our framework and results from MODIS GPP. The SIF is retrieved near the $\lambda = 740$ nm far-red peak in chlorophyll fluorescence emission from the Global Ozone Monitoring Experiment-2 (GOME-2) instrument onboard Eumetsat's MetOp-A satellite. The monthly SIF record (version 27, level 3) covering 2007–2016 was used in this study (Joiner, Yoshida, Guanter, & Middleton, 2016). SIF is an electromagnetic emission in the 650–800 nm range originating from plant photosynthetic machinery, and it is theoretically linearly correlated with the electron transport rate of photosynthetic activity (Zhang et al., 2014).

The eddy-covariance tower measurements from the FLUXNET2015 database (tier 1, Pastorello et al., 2017) were used in this study. FLUXNET is a global network of micrometeorological tower sites that use eddy covariance methods to measure the exchanges of carbon, water, and energy between terrestrial ecosystems and the atmosphere (Baldocchi et al., 2001). We used GPP estimates based on the flux partitioning approach proposed by Lasslop et al. (2010). A total of 92 sites (those with more than three site-year measurements) were selected for the evaluation of our $DOY_{P_{max}}$ framework spanning a large climatic and biome gradient (Figure S2a).

2.3 | Multiscale climate data

We used daily climate datasets provided by Global Modeling and Assimilation Office (GMAO) Reanalysis of NASA (Gelaro et al., 2017). The current version of GMAO is an hourly time step dataset generated by the Goddard Earth Observing System-5 (GEOS-5) data assimilation system. We aggregated the native hourly data into the daily scale to retrieve pixel-wise phases of climate variables. Surface air temperature and down-welling photosynthetically active radiation were employed in this analysis. Daily climate datasets were used to characterize $DOY_{T_{max}}$ and $DOY_{R_{max}}$. We also obtained potential evapotranspiration (PET) and actual evapotranspiration (AET) to quantify water availability on plant growth by calculating a ratio of AET to PET (RAP) (Prentice et al., 1992). Both AET and PET were obtained by Global Land Data Assimilation Systems (GLDAS, Version 2.1; Rodell et al., 2004). We characterized summer climate using mean temperature and RAP during June–August for investigating how $DOY_{P_{max}}$ positioning varies as functions of climate constraints, that is, temperature and water availability. For the tower-measured GPP, the ancillary microclimate datasets including air temperature and incoming radiation (photosynthetic photon flux density) simultaneously measured with GPP were additionally obtained.

2.4 | ESM simulated historical and future GPP

We also introduced a set of the most recent climate-carbon simulations of ESMs contributing to the fifth phase of the Coupled Model Intercomparison Project (CMIP5; Taylor, Stouffer, & Meehl, 2012). Seven ESMs, which are available at CMIP5 archive, were used in this study: NorESM1-M, MIROC-ESM, CanESM2, HadGEM2-ES, IPSL-CM5A-MR, MPI-ESM-MR, and CCSM4. The datasets provided monthly GPP output (1980–2099) for simulations of both Historical and Representative Concentration Pathway (RCP) 4.5 (Thomson et al., 2011). Data from the Historical and RCP4.5 scenario periods were combined to generate continuous variable fields from 1980 to 2099. All model outputs were processed at the native spatial resolutions and aggregated into regional scales (i.e., arctic, boreal, and temperate regions) for trend and correlation estimates.

2.5 | Timings of peak seasonal photosynthetic activity and climate

We extracted three metrics indicating a maximal state of seasonal photosynthetic activity ($DOY_{P_{max}}$), radiation ($DOY_{R_{max}}$),

and temperature ($DOY_{T_{max}}$) at two different scales: site and regional scale. For both scales, to reduce noise and maintain a distinct seasonal feature of GPP (or SIF) and climate datasets, the singular spectrum analysis was first implemented at yearly basis (Vautard, Yiou, & Ghil, 1992). The singular spectrum analysis is a nonparametric approach that does not need a priori specification of models of time series, thus it is data-adaptive. It first decomposes a time series into oscillatory components and noises according to the singular value decomposition, thereafter reconstructs specific components (i.e., seasonal signal) from the original time series. This nonparametric approach has been widely used to reconstruct the time series of GPP and other environmental variables by reducing their noise components (Keenan et al., 2014; Zhou et al., 2017). Time series of GPP and meteorological datasets were used to retrieve $DOY_{P_{max}}$, $DOY_{R_{max}}$, and $DOY_{T_{max}}$ on a yearly basis. Note that multiyear averaged daily GPP, radiation, and temperature time series were used for FLUXNET retrievals. For the case of monthly data (SIF and CMIP5 GPP), we assigned middle of the month as the day of the year for each month and then implemented the same procedures used in MODIS and FLUXNET. Finally, $\delta DOY_{P,R}$ (i.e., $DOY_{P_{max}} - DOY_{R_{max}}$) and $\delta DOY_{P,T}$ (i.e., $DOY_{P_{max}} - DOY_{T_{max}}$) were also calculated. We additionally retrieved pixel-wise growing season length from MODIS GPP by applying a fixed threshold, that is, 10% of the multiyear average maximum GPP (Zhou et al., 2017).

2.6 | Atmospheric CO₂ concentration and fluxes: zero-crossing date and seasonal amplitude

Daily atmospheric CO₂ concentration at Point Barrow (71.3°N, 156.6°W) was obtained from the in situ measurement dataset provided by the National Oceanic and Atmospheric Administration/Earth System Research Laboratory (NOAA/ESRL). The spring downward CO₂ zero-crossing date ($DOY_{zero-crossing}$) was extracted by following the approach described in Piao et al. (2008). We first detrended the interannual trend in the atmospheric CO₂ concentration with a quadratic polynomial curve, four harmonics in the seasonal function, and time-filtered residuals. We then used the harmonics plus the residuals (detrended CO₂ seasonal cycle) to define the downward CO₂ $do_{y_{zero-crossing}}$ as the day on which the detrended curve crossed the zero line from positive to negative. All aforementioned processes were achieved by the use of the standard package CCGCRV from NOAA/ESRL (Thoning, Tans, & Komhyr, 1989). We used $do_{y_{zero-crossing}}$ as an indicator of proximal $DOY_{P_{max}}$ for three reasons, although $DOY_{zero-crossing}$ is not an accurate term of peak photosynthesis timing. First, seasonal trajectory of GPP strongly governs changes in net biome productivity seasonality and its trend (Forkel et al., 2016; Ito et al., 2016). Second, $DOY_{zero-crossing}$ can be determined more accurately and it is roughly corresponding to the time of maximum carbon uptake by the biosphere (Ito et al., 2016). Third, a relative change in the phase of the cycle identified at one point (e.g., $DOY_{zero-crossing}$) will be matched by relative phase changes at all other points since the shape of the seasonal cycle does not change

significantly (Barichivich, Briffa, Osborn, Melvin, & Caesar, 2012). We further extracted the seasonal cycle amplitude (SCA) because its changes reflect vegetation GPP driven changes in net carbon uptake (Forkel et al., 2016).

We additionally used two gridded carbon fluxes from atmospheric CO₂ inversion products: the Copernicus Atmosphere Monitoring Service (CAM5, version v15r2, 1979–2015; Chevallier et al., 2010) and the Jena CarboScope (JENA, version s81_v3.8, 1981–2015; Rödenbeck, Houweling, Gloor, & Heimann, 2003). Atmospheric CO₂ inversions estimate net carbon exchange fluxes between surface and atmosphere by utilizing CO₂ concentrations at measurement sites, combined with an atmospheric transport model and prior information on fossil fuel carbon emissions and carbon exchange between the atmosphere and land (and ocean). We used daily mean net flux estimates on a spatial resolution of 3.75° latitude and 5° longitude (JENA) and 1.875° latitude and 3.75° longitude (CAM5) over the vegetated land surface. Both products were first aggregated into regional scales then DOY_{zero-crossing} and SCA of carbon fluxes were, respectively, extracted. Note that the flux amplitude is indirectly related to the amplitude in the atmospheric CO₂ concentration, as the atmospheric concentration is roughly the integral of the fluxes (Welp et al., 2016).

2.7 | Analytical approach

Based on the extracted MODIS DOY_{Pmax}, we first tested the validity of framework by relating it to summer climate conditions (i.e., temperature and water availability). The first principle we formulated for the framework justifies using summer season as a period when the primary climate constraint dictates vegetation photosynthetic seasonality, and therefore, DOY_{Pmax}. Both seasonal total (GPP_{Total}) and maximum GPP (GPP_{Pmax}) were calculated to investigate the spatial and temporal relations between DOY_{Pmax} and vegetation productivity. In order to capture the seasonal distribution of GPP with a simple metric, we evaluated the ratio (GPP_{Ratio}) of total GPP during the first half (January 1 to the long-term mean DOY_{Pmax}) to that of the whole year. Additionally, the length of growing season together with GPP_{Pmax} was considered to explain the observed pattern between DOY_{Pmax} and GPP_{Total} (e.g., Xia et al., 2015). All explored relationships were explained as functions of $\delta\text{DOY}_{P,R}$ and $\delta\text{DOY}_{P,T}$. Independent eddy-covariance tower GPP and GOME-2 SIF-based retrievals were used for further testing of the framework. Note that we limited the use of these independent data only for verifying the framework and not the change analysis because of limited temporal frequency and coverage of the data.

For the time series analysis, all trends in time series were computed as the slope of linear trends based on ordinary least squares regression. The significance of the trend was computed by using the nonparametric Mann–Kendall trend test. The standard error of the trend slope is also reported. We estimated the decadal trend based on the 5 year moving average approach to reduce the potential impact of first, last, and outlier points. The Kendall's rank correlation coefficient (r) was used to measure the

ordinal association between given two quantities. To understand how warming-induced DOY_{Pmax} shift has characterized northern land vegetation productivity, we investigated changes in temperature, DOY_{Pmax}, GPP_{Total}, and GPP_{Ratio}. This analysis was applied to both MODIS and ESMs-based retrievals. A trend in DOY_{zero-crossing} of three CO₂ data was, respectively, computed and correlation analysis between annual variations in DOY_{zero-crossing} and SCA was performed.

3 | RESULTS

3.1 | Spatial pattern of MODIS DOY_{Pmax} and its determinants

A distinct spatial gradient exists in DOY_{Pmax} and in its positioning with respect to the seasonal course of radiation and temperature (Figure 2a and Figure S2a,b). Overall, DOY_{Pmax} in arctic ecosystems is more closely aligned with DOY_{Tmax} ($\delta\text{DOY}_{P,T} = -9.3 \pm 5.5$ days, mean ± 1 SD) than DOY_{Rmax} ($\delta\text{DOY}_{P,R} = 29.1 \pm 8.5$ days), while in the boreal ecosystems it shows a much closer alignment with peak radiation levels ($\delta\text{DOY}_{P,T} = -13.3 \pm 5.4$ days, $\delta\text{DOY}_{P,R} = 12.9 \pm 10.5$ days). In the temperate regions, $\delta\text{DOY}_{P,R}$ is negative (-9.5 ± 27.0 days), that is, DOY_{Pmax} precedes DOY_{Rmax}. Temperature and water availability (i.e., RAP) limiting photosynthetic activity elucidate the observed regional variations in DOY_{Pmax} positioning. Every 1°C increase in temperature results in a $\delta\text{DOY}_{P,R}$ change of -5.7 ± 0.1 days (slope \pm SE, Figure 2b). In regions with negative $\delta\text{DOY}_{P,R}$, every 1% decrease in water availability results in a $\delta\text{DOY}_{P,R}$ change of -1.8 ± 0.1 days (Figure 2c). These results follow the two tenets of our framework, as outlined earlier complying with the laws of minimum (Blackman, 1905; Liebig, 1841; Sprengel, 1828). This suggests that the use of DOY_{Pmax} and its positioning in relation to DOY_{Rmax} and DOY_{Tmax} represents a feasible approach to assess plant's adaptive state to climatic constraints.

3.2 | Climate constraints, MODIS DOY_{Pmax}, and seasonal vegetation productivity

Emerging climatic constraints to plant growth are directly linked to changes in both GPP_{Total} (Figure 2d) and GPP_{Pmax} (Figure S2c). Regions with large GPP_{Pmax} are associated with tight synchrony between DOY_{Pmax} and DOY_{Rmax}, that is, both energy and water accessibility are least limiting (Bauerle et al., 2012). Ecosystems under either temperature- ($\delta\text{DOY}_{P,R} > 0$) or water-limited ($\delta\text{DOY}_{P,R} < 0$) environments show lower photosynthetic capacity by complying the general idea of climatic constraints to plant growth. Such interaction limiting photosynthetic activity is also tightly associated with growing season duration (Figure S2d). It is interesting to note that in areas with the largest GPP_{Total} (~ 1.07 kg C/m), DOY_{Pmax} slightly precedes DOY_{Rmax} ($\delta\text{DOY}_{P,R} \approx -7$ days) because of a joint control by growing season length and GPP_{Pmax} (Xia et al., 2015). The longest growing season duration (~ 6.5 months) is found when $\delta\text{DOY}_{P,R}$ is approximately equal to -17 days. This is known as “phenological trade-off,”

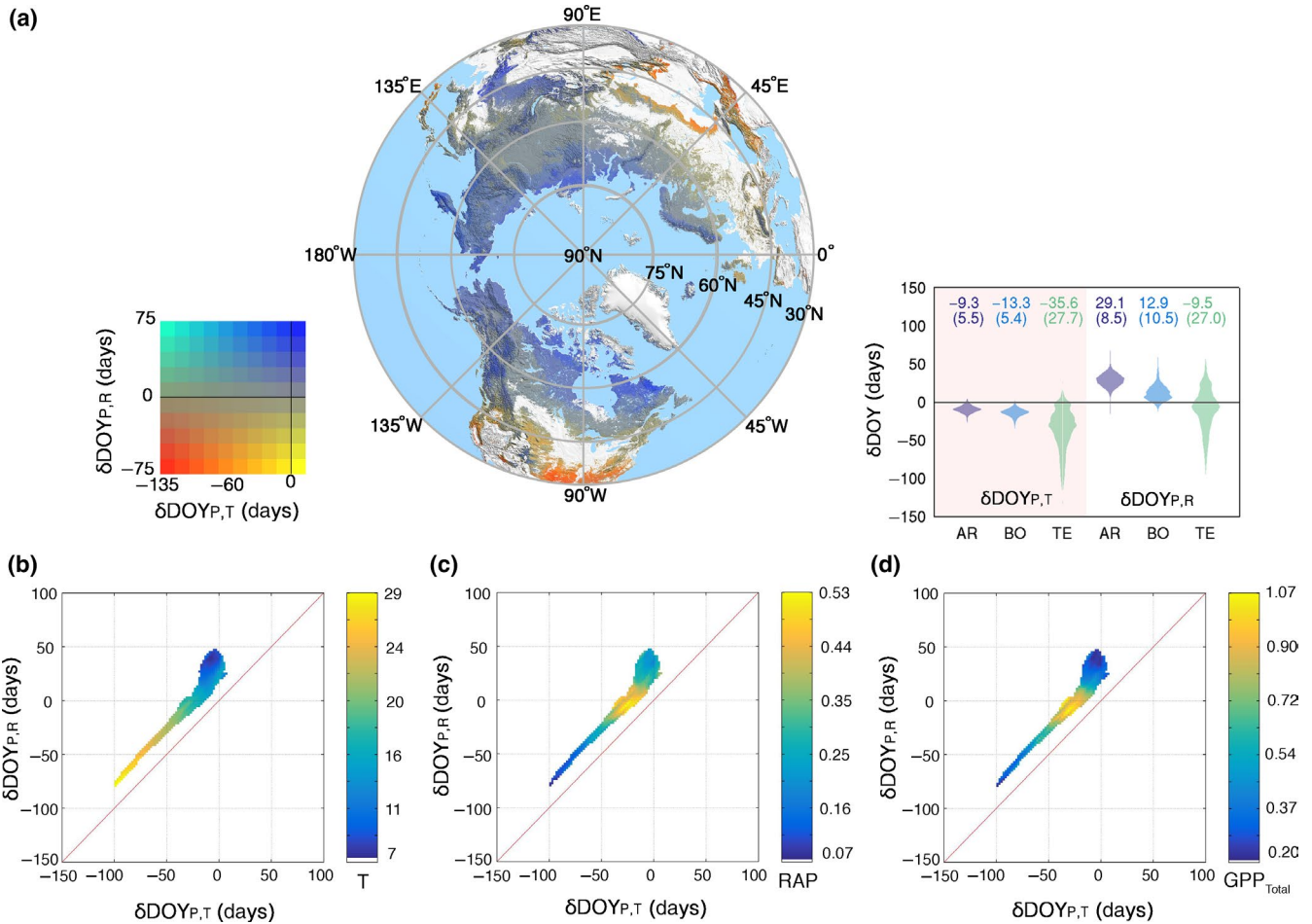


FIGURE 2 Relative positioning of peak photosynthetic activity timing with respect to the seasonal course of temperature and radiation, and its relation to climatic constraints and productivity. (a) Geographical distribution of $\delta\text{DOY}_{P,T}$ ($\text{DOY}_{P_{\text{max}}} - \text{DOY}_{T_{\text{max}}}$) and $\delta\text{DOY}_{P,R}$ ($\text{DOY}_{P_{\text{max}}} - \text{DOY}_{R_{\text{max}}}$) for northern ecosystems. Regional distribution of $\delta\text{DOY}_{P,T}$ and $\delta\text{DOY}_{P,R}$ over arctic (AR), boreal (BO), and temperate (TE) regions is given in the inset violin plot with mean and 1 SD (bracket). (b) Positioning of $\text{DOY}_{P_{\text{max}}}$ seen as the relation between $\delta\text{DOY}_{P,R}$ and $\delta\text{DOY}_{P,T}$, with respect to temperature ($^{\circ}\text{C}$). (c) Same as b but for water availability (i.e., RAP). (d) Same as (b) but for $\text{GPP}_{\text{Total}}$ (kg C/m^2). MODIS-derived outcomes are used for these panels

that is, a longer growing season imposed by warmer environment may result in a higher $\text{GPP}_{\text{Total}}$, but warmer and drier summers may suppress $\text{GPP}_{P_{\text{max}}}$, potentially offsetting the increased amount of $\text{GPP}_{\text{Total}}$ (Duvneek & Thompson, 2017).

3.3 | Confirmed patterns from two independent data: SIF and eddy-covariance tower GPP

Flux tower-measured GPP data from the eddy-covariance network and GOME-2 SIF confirm the above patterns observed in MODIS GPP products, thus lending further support for the proposed $\text{DOY}_{P_{\text{max}}}$ framework (Figure 3 and Figure S3).

3.4 | Changes in MODIS $\text{DOY}_{P_{\text{max}}}$ during last 17 years

Trend analyses reveal a widespread shift in MODIS $\text{DOY}_{P_{\text{max}}}$ toward earlier in the growing season dominating across 60.6% of the northern

vegetated area during last 17 years, and 32.8% of the area showing a significant negative trend ($p < 0.1$, Figure 4). These changes are seen across all three bioclimatic zones, that is, 31.9%, 38.7%, and 26.8% of the arctic, boreal, and temperate regions, respectively. At a hemispheric scale, we detected a significant trend toward an earlier peak photosynthetic rate of -1.66 ± 0.30 days/decade (slope \pm SE, $p < 0.001$) (Figure 5a), with regionally varying degree of advancing trends: a steeper change in the boreal region (-2.46 ± 0.47 days/decade, $p < 0.001$) relative to the temperate (-1.07 ± 0.26 days/decade, $p < 0.001$), and arctic regions (-1.09 ± 0.29 days/decade, $p < 0.001$). These changes are mostly associated with warming in the lands north of 30°N (Figures 4 and 5). The sensitivity of $\text{DOY}_{P_{\text{max}}}$ to warming was detected to be greater in the temperate (-4.27 ± 1.50 days/ $^{\circ}\text{C}$, $p < 0.001$) than in the arctic (-3.88 ± 1.29 days/ $^{\circ}\text{C}$, $p < 0.001$) and boreal (-3.91 ± 1.02 days/ $^{\circ}\text{C}$, $p < 0.001$) regions. Note that regionally varying warming rates (TE < AR < BO) lead to a different order of trend and sensitivity estimates. These changes in $\text{DOY}_{P_{\text{max}}}$ are interpreted as shifts in $\delta\text{DOY}_{P,R}$ across the arctic (-1.98 ± 7.30 days, mean \pm SD, t test, $p < 0.001$),

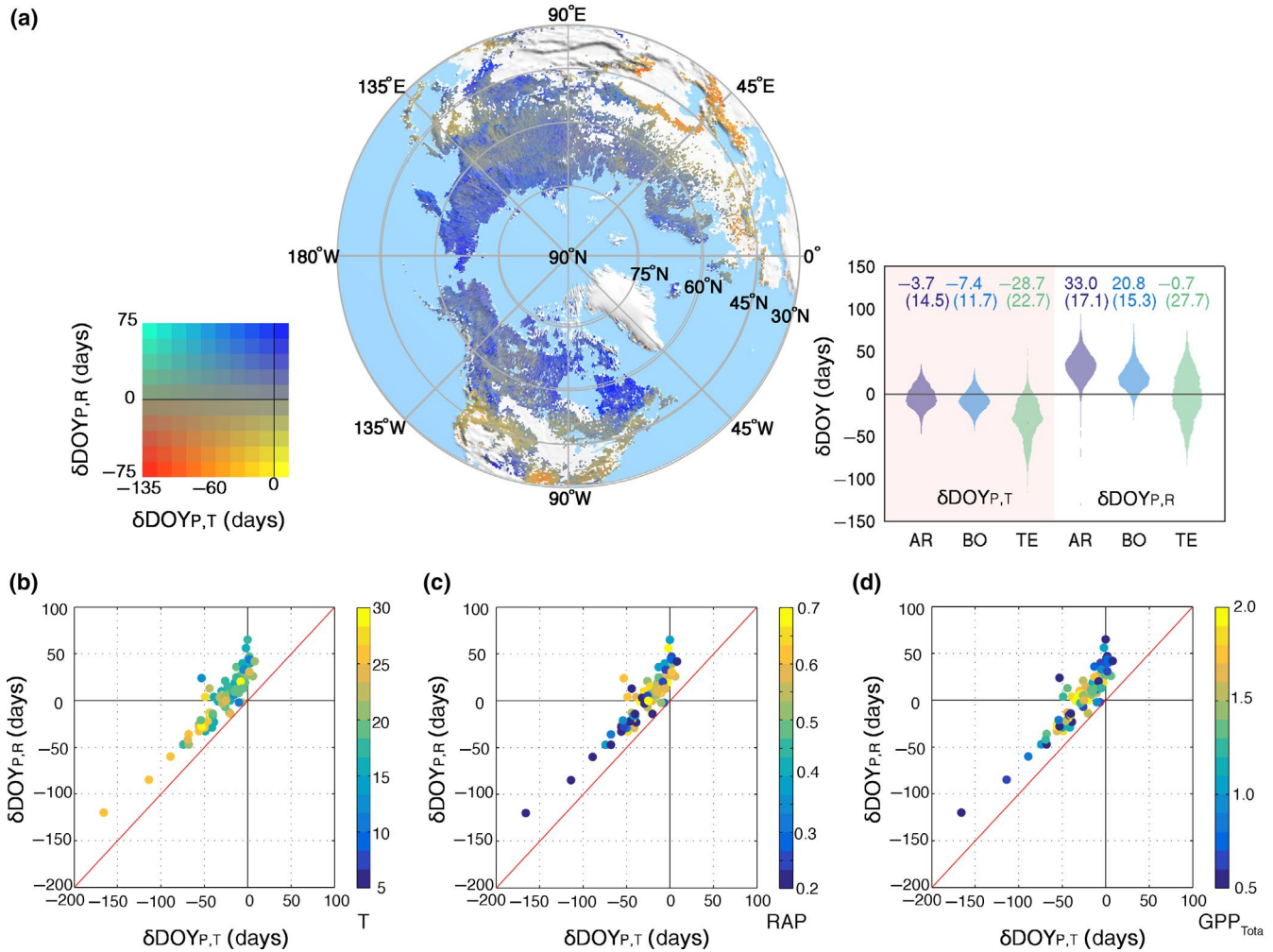


FIGURE 3 (a) Same as Figure 2a but for the independent satellite sun-induced fluorescence. (b)–(d) Same as Figure 2b–d but for the eddy covariance tower measurement. Total 92 FLUXNET sites (Figure S2a) were used and each dot represents a single site

boreal (-3.21 ± 5.83 days, $p < 0.001$), and temperate (-1.28 ± 12.76 days, $p < 0.001$) regions (Figure S4a,b). We find that the observed shift in DOY_{Pmax} is mainly responsible for the changes in $\delta\text{DOY}_{\text{P,R}}$ (and $\delta\text{DOY}_{\text{P,T}}$) because of relatively stable DOY_{Rmax} and DOY_{Tmax} changes (Figure S4 and Table S1). According to the principles in our framework, the shifts resulting a newly established photosynthetic seasonality with respect to seasonal climate factors imply changes in vegetation response to varying climatic constraints, that is, reduced relative importance of thermal constraint in the arctic and boreal vegetation while enhanced role of water availability in the temperate regions (Allen et al., 2010; Fu et al., 2015; Garonna et al., 2018; Piao et al., 2017; Figures 2c and 5). Note that some regions transitioning from positive to negative $\delta\text{DOY}_{\text{P,R}}$ might experience a critical tipping point where the ecosystems moves from temperature- toward water-limited ecosystems (Figure S5).

3.5 | Implications of changing MODIS DOY_{Pmax} on seasonal vegetation productivity

The changes in DOY_{Pmax} have regionally varying impacts on $\text{GPP}_{\text{Total}}$. An “earlier peak–larger productivity” pattern is dominant over the

arctic (-0.004 ± 0.002 kg C m^{-2} day^{-1} , slope \pm SE, $p < 0.05$) and boreal (-0.006 ± 0.002 kg C m^{-2} day^{-1} , $p < 0.05$) regions under a warming climate (Figure 5c). The framework proposed earlier informs that more favorable thermal conditions enable vegetation to increase its synchrony with seasonality in incoming radiation, with the seasonal course of photosynthetic activity tending toward the peak of radiation. Widely reported growing season extension (likely inferred from DOY_{Pmax} shift, Figure S2d) partly explains such “earlier peak–larger productivity” relation across the arctic and boreal regions (Park et al., 2016; Xu et al., 2013). Warmer temperatures might also enhance access to key nutrients (e.g., nitrogen), thus stimulating photosynthetic rates over the course of the entire growing season (Natali, Schuur, & Rubin, 2012). A weaker “earlier peak–less productivity” pattern in the temperate regions emerges due to complex climate–vegetation interactions (Figure 5c). Here, warmer conditions without moisture-stress result in an earlier DOY_{Pmax} and larger GPP_{Pmax} and $\text{GPP}_{\text{Total}}$. In other parts, where moisture stress is stronger, a significant decline in both GPP_{Pmax} and $\text{GPP}_{\text{Total}}$ is seen despite earlier DOY_{Pmax} (e.g., southwestern Eurasia) (Angert et al., 2005). In order to capture the seasonal distribution of GPP with a simple metric we evaluated the

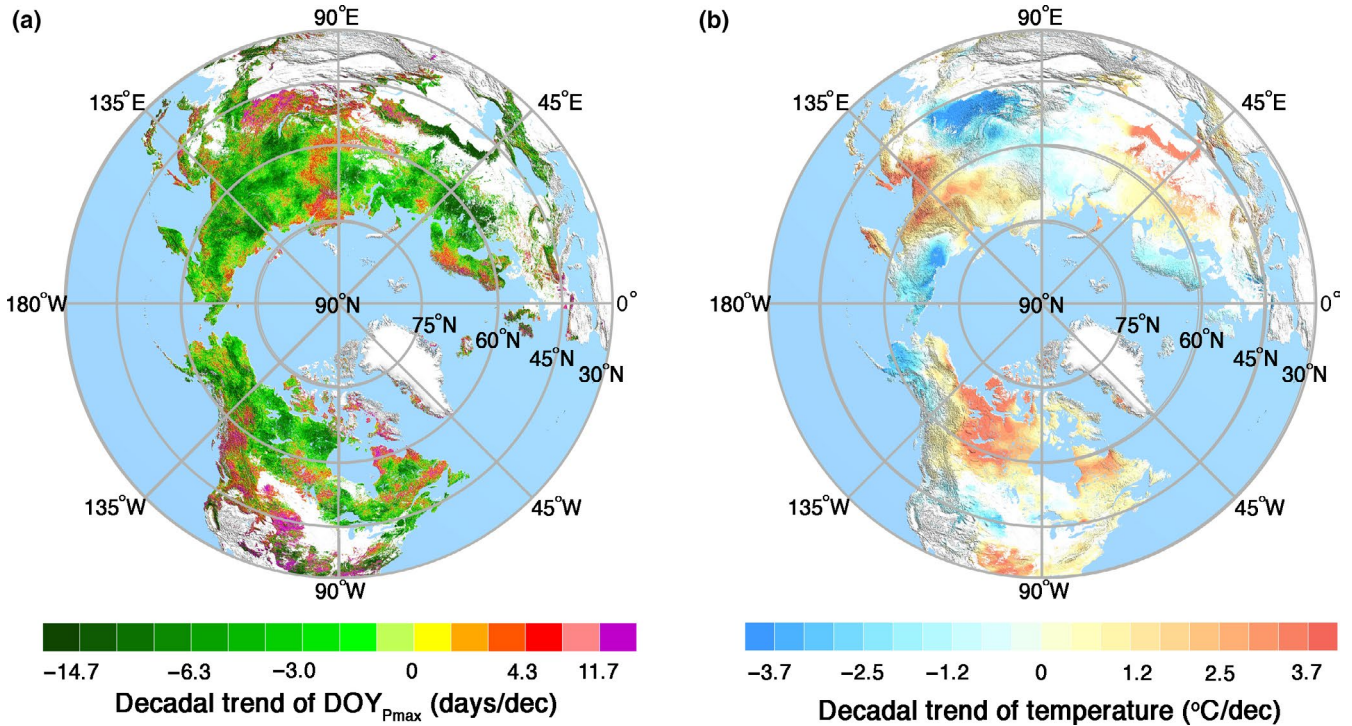


FIGURE 4 Spatial pattern of changes in DOY_{Pmax} and temperature during last 17 years (2000–2016). (a) Decadal trend of MODIS based DOY_{Pmax} over northern land during last 17 years. (b) Same as (a) but for summer temperature (June–August). The trend was derived based on ordinary least squares regression

ratio ($\text{GPP}_{\text{Ratio}}$) of total GPP during the first half (January 1 to the long-term mean DOY_{Pmax}) to that of the whole year. We find that DOY_{Pmax} occurring one day earlier in the season increases $\text{GPP}_{\text{Ratio}}$ by 0.28 ± 0.07 (temperate, slope \pm SE, $p < 0.001$) to $0.58 \pm 0.08\%$ (boreal, $p < 0.001$), clearly indicating an advance in gross carbon assimilation activity (Figure 5d; Duveneck & Thompson, 2017). This is an important indicator, as the photosynthetic activity is tightly linked to the atmosphere via carbon, water, and energy cycles. Thus, phase shifts in carbon, water, and energy cycles could be anticipated (Richardson et al., 2013).

3.6 | Changes in phase and amplitude of CO_2 seasonal cycle

We found that earlier peak photosynthesis and more carbon assimilation in the early part of the growing season altered the seasonal course of atmospheric CO_2 concentration. We used CO_2 observations from Point Barrow and two state-of-the-art CO_2 inversion datasets (i.e., CAMS and JENA). The springtime downward CO_2 zero-crossing date ($\text{DOY}_{\text{zero-crossing}}$) shows trends toward earlier downward $\text{DOY}_{\text{zero-crossing}}$ in the three CO_2 datasets (Figure 6a). The phase of atmospheric CO_2 at Point Barrow has advanced by 1.84 ± 0.20 days/decade (slope \pm SE, $p < 0.001$) since 1972. We also observe advancing trends but steeper changes in both CAMS (-2.42 ± 0.21 days/decade, $p < 0.001$) and JENA (-3.26 ± 0.21 days/decade, $p < 0.001$). This shift corroborates the advancing DOY_{Pmax} of gross photosynthetic activity observed

from space and shows the potential implications of enhanced gross carbon assimilation in the early growing season, that is, increased $\text{GPP}_{\text{Ratio}}$ (Barichivich et al., 2012; Randerson, Field, Fung, & Tans, 1999; Figure 5a,d). Furthermore, similar to what we observed in the analysis of DOY_{Pmax} and $\text{GPP}_{\text{Total}}$ (Figure 5c), SCA of three CO_2 data is negatively associated with $\text{DOY}_{\text{zero-crossing}}$ (Figure 6b). These phase shifts in the CO_2 data and their association with the enhanced seasonal amplitudes are in accordance with several observations (Barichivich et al., 2012; Graven et al., 2013; Randerson et al., 1999) and modeling studies (Duveneck & Thompson, 2017; Zhao & Zeng, 2014) suggesting enhanced peak photosynthetic activity and its advancing shift.

3.7 | Changes in ESMs simulated vegetation productivity and DOY_{Pmax}

We lastly ask whether state-of-the-art terrestrial biosphere models can reproduce the observed DOY_{Pmax} changes and their consequences under historical and future climate scenarios (Figure 7). The ESMs project an advancing DOY_{Pmax} across all northern bioclimatic zones for the period 1980–2030. We see a pattern of regional DOY_{Pmax} trends from ESMs analogous to satellite observations, that is, a strong trend for shifting to earlier in the season over the boreal (-0.94 ± 0.67 days/decade, mean \pm 1 SD across all ESMs), arctic (-0.86 ± 0.71 days/decade), and temperate (-0.58 ± 0.61 days/decade) regions. All models show a tightly linked negative relation between DOY_{Pmax} and $\text{GPP}_{\text{Total}}$, revealing

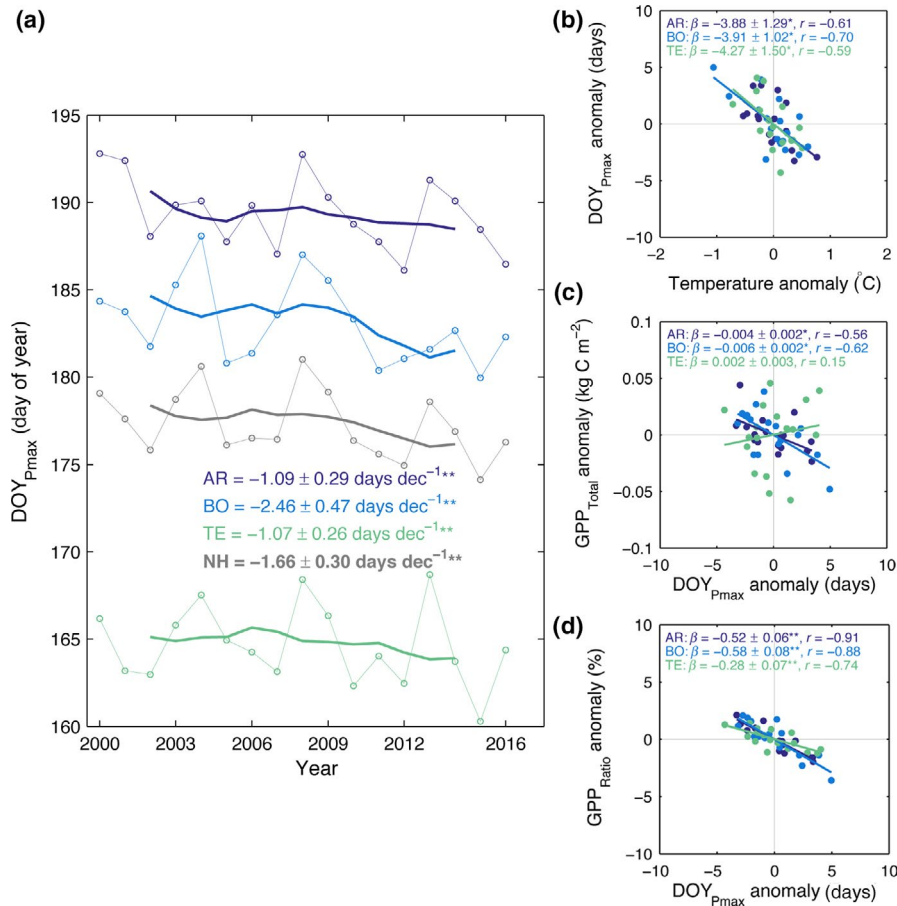


FIGURE 5 Changes in $DOY_{P_{max}}$ during last 17 years (2000–2016) and their implications on northern vegetation productivity. (a) Interannual variation of $DOY_{P_{max}}$ by regions (arctic: AR; boreal: BO; temperate: TE; Northern Hemisphere: NH) and its trend over last 17 years. The decadal trend is estimated based on the 5 year moving average approach to reduce the potential impact of first, last, and outlier points. Thin solid line with markers and thick solid line represent annual $DOY_{P_{max}}$ and 5 year moving average. Calculated trend (slope \pm SE) based on ordinary least squares regression is given with its significance level (double asterisks denote $p < 0.001$ and single asterisks denote $p < 0.05$). The significance was computed by using the nonparametric Mann–Kendall trend test. (b) Relation between regional $DOY_{P_{max}}$ and summer temperature (June–August) anomalies. (c, d) Same as b but for respective relation between $DOY_{P_{max}}$ and GPP_{Total} and $DOY_{P_{max}}$ and GPP_{Ratio} anomalies. The significance of the slope estimate ($\beta \pm$ SE) is denoted by double ($p < 0.001$) and single ($p < 0.05$) asterisks. The Kendall's rank correlation coefficient (r) between two variables is also given. Dark blue, light blue, green, and gray stand for AR, BO, TE, and NH, respectively

the “earlier peak-larger productivity” tendency as in current satellite observations. Particularly, temperature-constrained arctic and boreal regions have a tighter linkage between $DOY_{P_{max}}$ and GPP_{Total} than the warmer temperate regions. The shift in $DOY_{P_{max}}$ also increases the GPP_{Ratio} , indicating more carbon assimilation in the early part of the growing season than in the later period (Duveneck & Thompson, 2017; Zhao & Zeng, 2014). The pace of future (2050–2100) $DOY_{P_{max}}$ shift and its contribution to productivity is projected to continue, but to be slower and weaker than at present.

4 | DISCUSSION

Our analyses from long-term satellite records and ESMs reveal a widespread shift in $DOY_{P_{max}}$ toward earlier in the growing season.

The changes are associated with divergent consequences on GPP_{Total} depending on different states of climate constraints on plant growth. For high latitude arctic ecosystems, the advancement in $DOY_{P_{max}}$ likely continues in a warmer future climate as seen in the ESM simulations. Our framework translates the change into a continuous relaxation of temperature limit on arctic vegetation photosynthetic activity. A recent remote sensing based study supports our study by identifying a 16.4% decline in the area of vegetated land that is limited by temperature (Keenan & Riley, 2018). Yet, our framework suggests a reduction in the relative importance of temperature control on plant photosynthetic activity rather than a transitional state where other climate constraints primarily govern the ecosystem (Figure S4a). Indeed, long-term ground based studies in the Arctic tundra have shown that temperature is a primary driver of shrub growth and its expansion in arctic environment, while soil moisture controls the sensitivity of growth response to warming (Myers-Smith et al., 2015).

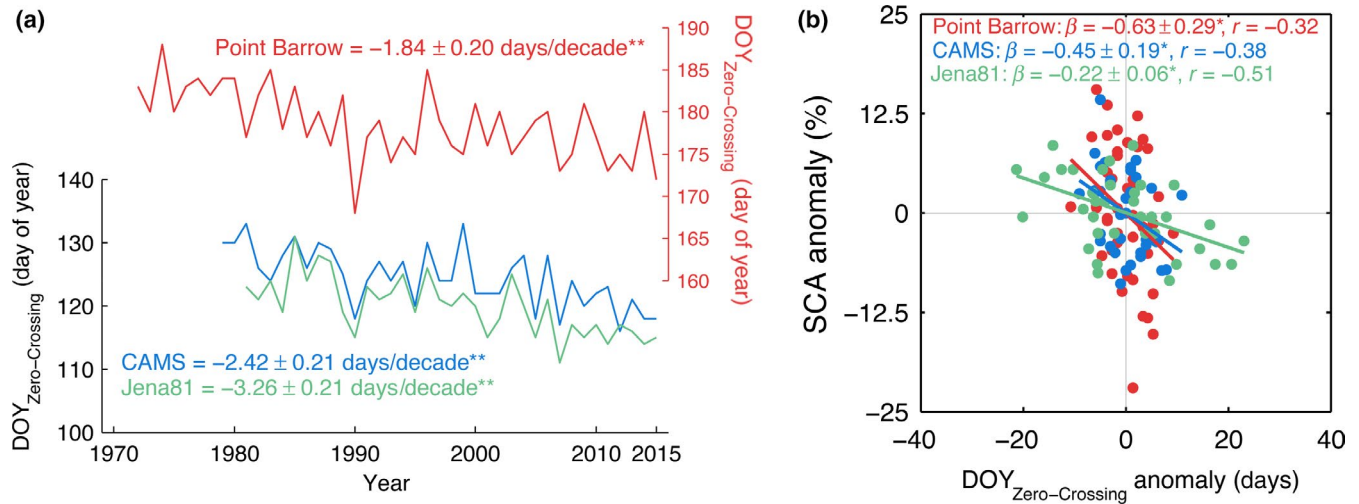


FIGURE 6 Analysis of atmospheric CO₂ concentration at Point Barrow and two CO₂ inversion estimates. (a) Time series of DOY_{zero-crossing} observed at Point Barrow atmospheric observatory and two independent CO₂ inversion datasets (CAM5 and JENA). Note that the CO₂ fluxes for DOY_{zero-crossing} retrieval of the inversion datasets are based on regionally integrated fluxes over the arctic and boreal zones, and all trend estimates are based on the 5 year moving average approach. Calculated trend (slope ± SE) based on ordinary least squares regression is given with its significance level (double asterisks denote $p < 0.001$ and single asterisks denote $p < 0.05$). The significance was computed by using the nonparametric Mann–Kendall trend test. (b) Relation between DOY_{zero-crossing} and seasonal cycle amplitude (SCA) of atmospheric CO₂ concentration and flux estimates. SCA anomaly was expressed as percentage of long-term mean. The significance of the slope estimate ($\beta \pm SE$) is denoted by double ($p < 0.001$) and single ($p < 0.05$) asterisks. The Kendall rank correlation coefficient (r) was used to measure the degree of association. Red, blue, and green stand for CO₂ data from Point Barrow, CAM5, and JENA, respectively

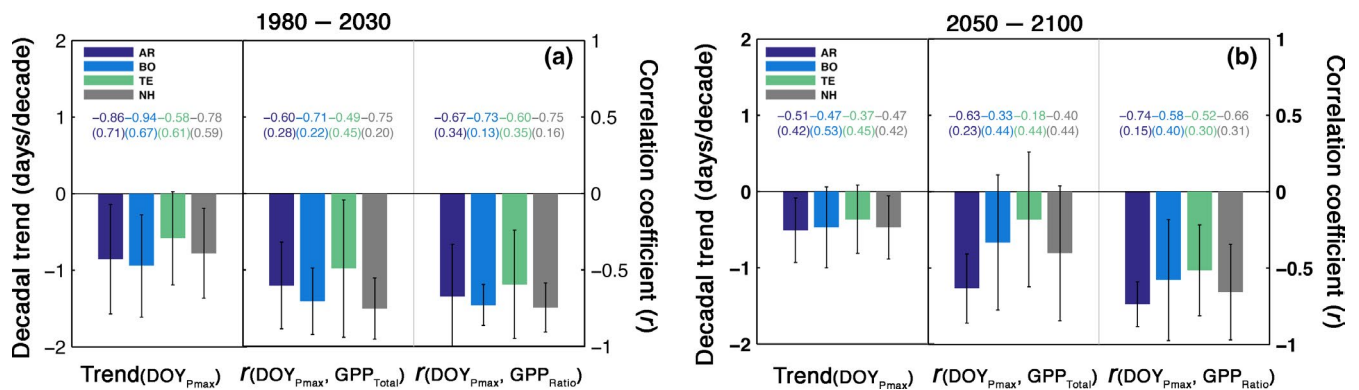


FIGURE 7 Analysis of multiple CMIP5 Earth system models (ESMs) during two separate periods: (a) 1980–2030 and (b) 2050–2100. Decadal trend of DOY_{Pmax} (left) and its association to GPP_{Total} (center) and GPP_{Ratio} (right) over northern lands inferred from the seven ESMs. Bar charts with error bars depict mean ± 1 SD across all ESMs. The Kendall rank correlation coefficient (r) was used to measure the degree of association. Dark blue, light blue, green, and gray stand for arctic (AR), boreal (BO), temperate (TE), and Northern Hemisphere (NH), respectively

Some of boreal ecosystems (northwest Russia and south Fennoscandia, south and southeast Canada) show a transition from positive to negative $\delta\text{DOY}_{P,R}$ during last two decades (Figure S5). This transition does not necessarily signify a decline of GPP_{Total} because of the “phenological trade-off” mechanism (Figure S2d). However, it is critical to monitor these ecosystems continuously because our framework suggests that there may be a tipping point where they move from temperature- toward water-limited ecosystems. That is, continuous warming and drying conditions may exacerbate moisture stress, and therefore, productivity reduction in these ecosystems. Interestingly, a recent tree-ring based study revealed that while

2°C of warming may increase overall forest productivity, additional warming could reverse this trend and lead to substantial moisture stress (D’Orangeville et al., 2018). Also, multiple warming experiments confirm the dynamism of climate constraints on plant growth in the southern boreal forest and highlight the vulnerability of the ecosystem to excess warming and drying (e.g., Reich et al., 2018).

Warmer and drier conditions over temperate vegetation, where negative $\delta\text{DOY}_{P,R}$ is dominant, generally result in a decrease of plant growth. Widespread increase of tree mortality of this susceptible ecosystem to worsening moisture stress has been reported (Allen et al., 2010). Most epidemic climate-induced tree mortality events occurs

over the regions where water availability is the primary climate constraint on photosynthetic activity (i.e., $\delta\text{DOY}_{\text{P,R}} < 0$, see Figure S5). It agrees with the “earlier peak–less productivity” pattern in warmer temperate vegetation from MODIS data. However, the relation was not reproduced by the ESMs. The models projected that warming-induced earlier peak photosynthesis leads to an enhanced seasonal total productivity (Figure 7a). Recent studies have shown that current terrestrial carbon cycle models substantially overestimate (underestimate) positive (negative) effects associated with warming (Buermann et al., 2018). It is possibly because these models inadequately capture the effects of the seasonal build-up of water stress on seasonal vegetation growth.

Our analyses of $\text{DOY}_{\text{zero-crossing}}$ and SCA confirm the advancing and enhancing CO_2 seasonal cycle in northern lands (Barichivich et al., 2012; Forkel et al., 2016; Graven et al., 2013). An additional remark made here for ongoing changes in biosphere–atmosphere interaction is an asymmetric enhancement of terrestrial photosynthetic activity. We find a widespread warming-induced DOY_{Pmax} advancement and $\text{GPP}_{\text{Total}}$ increase across northern lands, and these changes possibly play a role in ongoing shift and amplified atmospheric CO_2 seasonal cycle. This is because peak photosynthesis rate explains about 78% of the variation of seasonal total productivity and only 21% can be explained by growing season changes (Xia et al., 2015). Our results confirm that a larger beneficial carbon uptake from an extended growing season is dominated by the later part of spring, when more fully developed leaf area with more favorable light and temperature is available for photosynthetic activity (Keenan et al., 2014). Together with these earlier studies, our findings suggest that an intraseasonal scale may provide a possible but overlooked mechanism for the changes in atmospheric CO_2 seasonal cycle. Furthermore, the observed shift in the relative importance of climate constraints on plant growth may be a possible mechanism for the recently reported weakening temperature controls on spring carbon uptake across northern lands (Piao et al., 2017).

Furthermore, our framework also gives insight into the changes in growing season duration and its implication on carbon cycle. As described in Figure 1, thermal inertia induced decoupling of radiation and temperature characterizes a unique seasonal climate environment to local vegetation. For temperature-constrained ecosystems (see Case 2 in Figure 1), DOY_{Tmax} -ward DOY_{Pmax} positioning leads to strong temperature dependence in spring photosynthesis while light availability emerges as an important controller in autumnal activity (Garonna et al., 2018). This intrinsic physical environment indicates contrasting responses of photosynthetic activity to spring versus autumn warming. In this cold environment, spring warming generally stimulates carbon uptake by extending onset of growing season (Pulliainen et al., 2017). In contrast, autumnal growing season extension and its photosynthetic carbon gain will be strongly limited by radiation (Bauerle et al., 2012). Multiple studies have reported that the increase of autumn temperature results in net carbon loss indicating more respiratory loss than photosynthetic gain in northern lands (Commane et al.,

2017; Piao et al., 2008). These contrasting seasonal responses also partially explain the observed and projected asymmetric enhancement of photosynthetic activity and carbon cycles in northern lands. However, further studies will be required to identify which case the autumn growing season extension can lead to increased photosynthesis sufficient to balance the higher respiration carbon loss.

Most of ESMs as well as MODIS GPP estimate used in this study do not include photosynthetic temperature acclimation process. This physiological adjustment is commonly observed as a shift in the optimum temperature for carbon assimilation rate by modulating local plant's metabolism (Yamori, Hikosaka, & Way, 2014). We expect that taking the photosynthetic thermal acclimation likely lead to a slightly closer alignment between DOY_{Pmax} and DOY_{Rmax} than the one without the process. It also may reduce the observed DOY_{Pmax} sensitivity to warming (Smith, Malyshev, Shevliakova, Kattge, & Dukes, 2016). Nevertheless, we believe that the proposed DOY_{Pmax} framework and its changes are valid because of multiple evidence from independent datasets in this work (Figure 3 and Figure S3) and previous studies (Buitenwerf et al., 2015; Gonsamo et al., 2018; Rotenberg & Yakir, 2010). Interestingly, dendrometer-based intra-annual tree growth studies also support our framework (e.g., Rossi et al., 2006). Ongoing efforts for advancements in modeling communities (Rogers et al., 2017) will help to deploy temperature acclimation modules in ESMs and thus better understandings on seasonal photosynthesis and DOY_{Pmax} changes are expected.

In summary, our results highlight a significant shift in terrestrial photosynthetic activity north of 30°N , implying a constantly adapting state of climatic constraints on plant growth. A consensus of multiple Earth observations and ESMs on this change imbues confidence in our findings. This is a critical development because the shifts in peak photosynthesis may cause cascading perturbations in Earth system components that include carbon, water, and energy balances (Richardson et al., 2013), as well as ecological interactions (Walther, 2010). The framework proposed here is one of the first attempts to introduce the time of peak photosynthesis as an indicator of a plant's adaptive state to climatic constraints, and provides a simplified yet realistic framework for the complex mechanisms by which various climatic factors constrain plant growth.

ACKNOWLEDGEMENTS

We thankfully acknowledge FLUXNET, CMIP5, and MODIS Science team members for their data making available. We also like to thank Christian Rödenbeck and Chevallier Frederic for sharing the JENA and CAMS CO_2 inversion data. Further, we thank Joanna Joiner for providing the GOME-2 SIF data. This work was funded by NASA Earth Science Directorate (grants NNX16AO34H, NNX14AP80A and NNX14AI71G) and the Research Council of Norway (grants 287402 and 270992). A Natural Environment Research Council Independent Research Fellowship (NE/L011859/1) funded M.M.-F.'s contribution.

AUTHOR CONTRIBUTIONS

TP and RBM designed the research; TP performed the analysis and wrote the draft; and all the authors contributed to the interpretation of the results and the writing of the paper.

ORCID

Taejin Park  <https://orcid.org/0000-0003-0698-6942>

Marc Macias-Fauria  <https://orcid.org/0000-0002-8438-2223>

Hans Tømmervik  <https://orcid.org/0000-0001-7273-1695>

Shilong Piao  <https://orcid.org/0000-0001-8057-2292>

REFERENCES

- Allen, C. D., Macalady, A. K., Chenchouni, H., Bachelet, D., McDowell, N., Vennetier, M., ... Cobb, N. (2010). A global overview of drought and heat-induced tree mortality reveals emerging climate change risks for forests. *Forest Ecology and Management*, 259(4), 660–684. <https://doi.org/10.1016/j.foreco.2009.09.001>
- Angert, A., Biraud, S., Bonfils, C., Henning, C. C., Buermann, W., Pinzon, J., ... Fung, I. (2005). Drier summers cancel out the CO₂ uptake enhancement induced by warmer springs. *Proceedings of the National Academy of Sciences of the United States of America*, 102(31), 10823–10827. <https://doi.org/10.1073/pnas.0501647102>
- Baldocchi, D., Falge, E., Gu, L., Olson, R., Hollinger, D., Running, S., ... Wofsy, S. (2001). FLUXNET: A new tool to study the temporal and spatial variability of ecosystem-scale carbon dioxide, water vapor, and energy flux densities. *Bulletin of the American Meteorological Society*, 82(11), 2415–2434. [https://doi.org/10.1175/1520-0477\(2001\)082<2415:FANTTS>2.3.CO;2](https://doi.org/10.1175/1520-0477(2001)082<2415:FANTTS>2.3.CO;2)
- Barichivich, J., Briffa, K., Myneni, R., Schrier, G., Dorigo, W., Tucker, C., ... Melvin, T. (2014). Temperature and snow-mediated moisture controls of summer photosynthetic activity in northern terrestrial ecosystems between 1982 and 2011. *Remote Sensing*, 6(2), 1390–1431. <https://doi.org/10.3390/rs6021390>
- Barichivich, J., Briffa, K. R., Osborn, T. J., Melvin, T. M., & Caesar, J. (2012). Thermal growing season and timing of biospheric carbon uptake across the Northern Hemisphere. *Global Biogeochemical Cycles*, 26(4). <https://doi.org/10.1029/2012GB004312>
- Bauerle, W. L., Oren, R., Way, D. A., Qian, S. S., Stoy, P. C., Thornton, P. E., ... Reynolds, R. F. (2012). Photoperiodic regulation of the seasonal pattern of photosynthetic capacity and the implications for carbon cycling. *Proceedings of the National Academy of Sciences of the United States of America*, 109(22), 8612–8617. <https://doi.org/10.1073/pnas.1119131109>
- Blackman, F. F. (1905). Optima and limiting factors. *Annals of Botany*, 19(74), 281–295. <https://doi.org/10.1093/oxfordjournals.aob.a089000>
- Buermann, W., Forkel, M., O'Sullivan, M., Sitch, S., Friedlingstein, P., Haverd, V., ... Richardson, A. D. (2018). Widespread seasonal compensation effects of spring warming on northern plant productivity. *Nature*, 562(7725), 110–114. <https://doi.org/10.1038/s41586-018-0555-7>
- Buitenwerf, R., Rose, L., & Higgins, S. I. (2015). Three decades of multi-dimensional change in global leaf phenology. *Nature Climate Change*, 5(4), 364–368. <https://doi.org/10.1038/nclimate2533>
- Chevallier, F., Ciais, P., Conway, T., Aalto, T., Anderson, B., Bousquet, P., ... Fröhlich, M. (2010). CO₂ surface fluxes at grid point scale estimated from a global 21 year reanalysis of atmospheric measurements. *Journal of Geophysical Research: Atmospheres*, 115(D21).
- Chuine, I., & Beaubien, E. G. (2001). Phenology is a major determinant of tree species range. *Ecology Letters*, 4(5), 500–510. <https://doi.org/10.1046/j.1461-0248.2001.00261.x>
- Commane, R., Lindaas, J., Benmergui, J., Luus, K. A., Chang, R.-W., Daube, B. C., ... Wofsy, S. C. (2017). Carbon dioxide sources from Alaska driven by increasing early winter respiration from Arctic tundra. *Proceedings of the National Academy of Sciences of the United States of America*, 114(21), 5361–5366. <https://doi.org/10.1073/pnas.1618567114>
- D'Orangeville, L., Houle, D., Duchesne, L., Phillips, R. P., Bergeron, Y., & Kneeshaw, D. (2018). Beneficial effects of climate warming on boreal tree growth may be transitory. *Nature Communications*, 9(1), 3213. <https://doi.org/10.1038/s41467-018-05705-4>
- Duveneck, M. J., & Thompson, J. R. (2017). Climate change imposes phenological trade-offs on forest net primary productivity. *Journal of Geophysical Research: Biogeosciences*, 122(9), 2298–2313. <https://doi.org/10.1002/2017JG004025>
- Eagleson, P. S. (2005). *Ecohydrology: Darwinian expression of vegetation form and function*. Cambridge: Cambridge University Press.
- Forkel, M., Carvalhais, N., Rödenbeck, C., Keeling, R., Heimann, M., Thonicke, K., ... Reichstein, M. (2016). Enhanced seasonal CO₂ exchange caused by amplified plant productivity in northern ecosystems. *Science*, 351(6274), 696–699.
- Friedl, M. A., Sulla-Menashe, D., Tan, B., Schneider, A., Ramankutty, N., Sibley, A., & Huang, X. (2010). MODIS Collection 5 global land cover: Algorithm refinements and characterization of new datasets. *Remote Sensing of Environment*, 114(1), 168–182. <https://doi.org/10.1016/j.rse.2009.08.016>
- Fritz, S., See, L., McCallum, I., You, L., Bun, A., Moltchanova, E., ... Obersteiner, M. (2015). Mapping global cropland and field size. *Global Change Biology*, 21(5), 1980–1992. <https://doi.org/10.1111/gcb.12838>
- Fu, Y. H., Zhao, H., Piao, S., Peaucelle, M., Peng, S., Zhou, G., ... Janssens, I. A. (2015). Declining global warming effects on the phenology of spring leaf unfolding. *Nature*, 526(7571), 104. <https://doi.org/10.1038/nature15402>
- Garonna, I., de Jong, R., Stöckli, R., Schmid, B., Schenkel, D., Schimel, D., & Schaepman, M. E. (2018). Shifting relative importance of climatic constraints on land surface phenology. *Environmental Research Letters*, 13(2), 024025. <https://doi.org/10.1088/1748-9326/aaa17b>
- Gelaro, R., McCarty, W., Suárez, M. J., Todling, R., Molod, A., Takacs, L., ... Zhao, B. (2017). The modern-era retrospective analysis for research and applications, version 2 (MERRA-2). *Journal of Climate*, 30(14), 5419–5454. <https://doi.org/10.1175/JCLI-D-16-0758.1>
- Gonsamo, A., Chen, J. M., & Ooi, Y. W. (2018). Peak season plant activity shift towards spring is reflected by increasing carbon uptake by extratropical ecosystems. *Global Change Biology*, 24(5), 2117–2128. <https://doi.org/10.1111/gcb.14001>
- Graven, H. D., Keeling, R. F., Piper, S. C., Patra, P. K., Stephens, B. B., Wofsy, S. C., ... Bent, J. D. (2013). Enhanced seasonal exchange of CO₂ by northern ecosystems since 1960. *Science*, 341(6150), 1085–1089. <https://doi.org/10.1126/science.1239207>
- Heinsch, F. A., Zhao, M., Running, S. W., Kimball, J. S., Nemani, R. R., Davis, K. J., ... Flanagan, L. B. (2006). Evaluation of remote sensing based terrestrial productivity from MODIS using regional tower eddy flux network observations. *IEEE Transactions on Geoscience and Remote Sensing*, 44(7), 1908–1925. <https://doi.org/10.1109/TGRS.2005.853936>
- Ito, A., Inatomi, M., Huntzinger, D. N., Schwalm, C., Michalak, A. M., Cook, R., ... Post, W. M. (2016). Decadal trends in the seasonal-cycle amplitude of terrestrial CO₂ exchange resulting from the ensemble of terrestrial biosphere models. *Tellus B: Chemical and Physical Meteorology*, 68(1), 28968.
- Joiner, J., Yoshida, Y., Guanter, L., & Middleton, E. M. (2016). New methods for the retrieval of chlorophyll red fluorescence from hyperspectral

- satellite instruments: Simulations and application to GOME-2 and SCIAMACHY. *Atmospheric Measurement Techniques*, 9(8).
- Jolly, W. M., Nemani, R., & Running, S. W. (2005). A generalized, bioclimatic index to predict foliar phenology in response to climate. *Global Change Biology*, 11(4), 619–632. <https://doi.org/10.1111/j.1365-2486.2005.00930.x>
- Keenan, T. F., Gray, J., Friedl, M. A., Toomey, M., Bohrer, G., Hollinger, D. Y., ... Richardson, A. D. (2014). Net carbon uptake has increased through warming-induced changes in temperate forest phenology. *Nature Climate Change*, 4(7), 598–604. <https://doi.org/10.1038/nclimate2253>
- Keenan, T., & Riley, W. (2018). Greening of the land surface in the world's cold regions consistent with recent warming. *Nature Climate Change*, 8(9), 825. <https://doi.org/10.1038/s41558-018-0258-y>
- Lasslop, G., Reichstein, M., Papale, D., Richardson, A. D., Arneeth, A., Barr, A., ... Wohlfahrt, G. (2010). Separation of net ecosystem exchange into assimilation and respiration using a light response curve approach: Critical issues and global evaluation. *Global Change Biology*, 16(1), 187–208. <https://doi.org/10.1111/j.1365-2486.2009.02041.x>
- Liebig, J. (1841). *Organic chemistry in its applications to agriculture and physiology*. J. Owen. London: Taylor and Walton.
- Myers-Smith, I. H., Elmendorf, S. C., Beck, P. S. A., Wilkening, M., Hallinger, M., Blok, D., ... Vellend, M. (2015). Climate sensitivity of shrub growth across the tundra biome. *Nature Climate Change*, 5(9), 887. <https://doi.org/10.1038/nclimate2697>
- Natali, S. M., Schuur, E. A., & Rubin, R. L. (2012). Increased plant productivity in Alaskan tundra as a result of experimental warming of soil and permafrost. *Journal of Ecology*, 100(2), 488–498. <https://doi.org/10.1111/j.1365-2745.2011.01925.x>
- Nemani, R. R., Keeling, C. D., Hashimoto, H., Jolly, W. M., Piper, S. C., Tucker, C. J., ... Running, S. W. (2003). Climate-driven increases in global terrestrial net primary production from 1982 to 1999. *Science*, 300(5625), 1560–1563.
- Olson, D. M., Dinerstein, E., Wikramanayake, E. D., Burgess, N. D., Powell, G. V. N., Underwood, E. C., ... Kassem, K. R. (2001). Terrestrial ecoregions of the world: A new map of life on earth: A new global map of terrestrial ecoregions provides an innovative tool for conserving biodiversity. *BioScience*, 51(11), 933–938. [https://doi.org/10.1641/0006-3568\(2001\)051\[0933:TEOTWA\]2.0.CO;2](https://doi.org/10.1641/0006-3568(2001)051[0933:TEOTWA]2.0.CO;2)
- Park, T., Ganguly, S., Tømmervik, H., Euskirchen, E. S., Høgda, K.-A., Karlsen, S. R., ... Myneni, R. B. (2016). Changes in growing season duration and productivity of northern vegetation inferred from long-term remote sensing data. *Environmental Research Letters*, 11(8), 084001. <https://doi.org/10.1088/1748-9326/11/8/084001>
- Parmesan, C., & Yohe, G. (2003). A globally coherent fingerprint of climate change impacts across natural systems. *Nature*, 421(6918), 37. <https://doi.org/10.1038/nature01286>
- Pastorello, G., Papale, D., Chu, H., Trotta, C., Agarwal, D., Canfora, E., ... Torn, M. (2017). A new data set to keep a sharper eye on land-air exchanges. *Eos, Transactions American Geophysical Union (Online)*, 98(8). <https://doi.org/10.1029/2017EO071597>
- Peng, C., Ma, Z., Lei, X., Zhu, Q., Chen, H., Wang, W., ... Zhou, X. (2011). A drought-induced pervasive increase in tree mortality across Canada's boreal forests. *Nature Climate Change*, 1(9), 467. <https://doi.org/10.1038/nclimate1293>
- Piao, S., Ciais, P., Friedlingstein, P., Peylin, P., Reichstein, M., Luysaert, S., ... Chen, A. (2008). Net carbon dioxide losses of northern ecosystems in response to autumn warming. *Nature*, 451(7174), 49–52.
- Piao, S., Liu, Z., Wang, T., Peng, S., Ciais, P., Huang, M., ... Tans, P. P. (2017). Weakening temperature control on the interannual variations of spring carbon uptake across northern lands. *Nature Climate Change*, 7(5), 359–363. <https://doi.org/10.1038/nclimate3277>
- Prentice, I. C., Cramer, W., Harrison, S. P., Leemans, R., Monserud, R. A., & Solomon, A. M. (1992). Special paper: A global biome model based on plant physiology and dominance, soil properties and climate. *Journal of Biogeography*, 117–134. <https://doi.org/10.2307/2845499>
- Pulliaainen, J., Aurela, M., Laurila, T., Aalto, T., Takala, M., Salminen, M., ... Vesala, T. (2017). Early snowmelt significantly enhances boreal springtime carbon uptake. *Proceedings of the National Academy of Sciences of the United States of America*, 114(42), 11081–11086. <https://doi.org/10.1073/pnas.1707889114>
- Randerson, J., Field, C., Fung, I., & Tans, P. (1999). Increases in early season ecosystem uptake explain recent changes in the seasonal cycle of atmospheric CO₂ at high northern latitudes. *Geophysical Research Letters*, 26(17), 2765–2768.
- Reich, P. B., Sendall, K. M., Stefanski, A., Rich, R. L., Hobbie, S. E., & Montgomery, R. A. (2018). Effects of climate warming on photosynthesis in boreal tree species depend on soil moisture. *Nature*, 562(7726), 263. <https://doi.org/10.1038/s41586-018-0582-4>
- Richardson, A. D., Black, T. A., Ciais, P., Delbart, N., Friedl, M. A., Gobron, N., ... Migliavacca, M. (2010). Influence of spring and autumn phenological transitions on forest ecosystem productivity. *Philosophical Transactions of the Royal Society of London B: Biological Sciences*, 365(1555), 3227–3246.
- Richardson, A. D., Keenan, T. F., Migliavacca, M., Ryu, Y., Sonnentag, O., & Toomey, M. (2013). Climate change, phenology, and phenological control of vegetation feedbacks to the climate system. *Agricultural and Forest Meteorology*, 169, 156–173. <https://doi.org/10.1016/j.agrformet.2012.09.012>
- Rodell, M., Houser, P. R., Jambor, U., Gottschalk, J., Mitchell, K., Meng, C.-J., ... Toll, D. (2004). The global land data assimilation system. *Bulletin of the American Meteorological Society*, 85(3), 381–394. <https://doi.org/10.1175/BAMS-85-3-381>
- Rödenbeck, C., Houweling, S., Gloor, M., & Heimann, M. (2003). CO₂ flux history 1982–2001 inferred from atmospheric data using a global inversion of atmospheric transport. *Atmospheric Chemistry and Physics*, 3(6), 1919–1964.
- Rogers, A., Medlyn, B. E., Dukes, J. S., Bonan, G., von Caemmerer, S., Dietze, M. C., ... Zaehle, S. (2017). A roadmap for improving the representation of photosynthesis in Earth system models. *New Phytologist*, 213(1), 22–42. <https://doi.org/10.1111/nph.14283>
- Rossi, S., Deslauriers, A., Anfodillo, T., Morin, H., Saracino, A., Motta, R., ... Borghetti, M. (2006). Conifers in cold environments synchronize maximum growth rate of tree-ring formation with day length. *New Phytologist*, 170(2), 301–310. <https://doi.org/10.1111/j.1469-8137.2006.01660.x>
- Rotenberg, E., & Yakir, D. (2010). Contribution of semi-arid forests to the climate system. *Science*, 327(5964), 451–454.
- Running, S., Mu, Q., & Zhao, M. (2015). MOD17A2H MODIS/terra gross primary productivity 8-day L4 global 500m SIN grid V006. NASA EOSDIS Land Processes DAAC.
- Smith, N. G., Malyshev, S. L., Shevliakova, E., Kattge, J., & Dukes, J. S. (2016). Foliar temperature acclimation reduces simulated carbon sensitivity to climate. *Nature Climate Change*, 6(4), 407. <https://doi.org/10.1038/nclimate2878>
- Sprengel, C. (1828). Von den Substanzen der Ackerkrume und des Untergrundes [About the substances in the plow layer and the subsoil]. *Journal für Technische und Oekonomische Chemie*, 2, 397–421. (in German)
- Taylor, K. E., Stouffer, R. J., & Meehl, G. A. (2012). An overview of CMIP5 and the experiment design. *Bulletin of the American Meteorological Society*, 93(4), 485–498. <https://doi.org/10.1175/BAMS-D-11-00094.1>
- Thomson, A. M., Calvin, K. V., Smith, S. J., Kyle, G. P., Volke, A., Patel, P., ... Clarke, L. E. (2011). RCP4. 5: A pathway for stabilization of radiative forcing by 2100. *Climatic Change*, 109(1–2), 77.
- Thoning, K. W., Tans, P. P., & Komhyr, W. D. (1989). Atmospheric carbon dioxide at Mauna Loa Observatory: 2. Analysis of the NOAA GMCC

- data, 1974–1985. *Journal of Geophysical Research: Atmospheres*, 94(D6), 8549–8565.
- Vautard, R., Yiou, P., & Ghil, M. (1992). Singular-spectrum analysis: A toolkit for short, noisy chaotic signals. *Physica D: Nonlinear Phenomena*, 58(1–4), 95–126. [https://doi.org/10.1016/0167-2789\(92\)90103-T](https://doi.org/10.1016/0167-2789(92)90103-T)
- Walther, G. R. (2010). Community and ecosystem responses to recent climate change. *Philosophical Transactions of the Royal Society of London B: Biological Sciences*, 365(1549), 2019–2024.
- Welp, L. R., Patra, P. K., Rödenbeck, C., Nemani, R., Bi, J., Piper, S. C., & Keeling, R. F. (2016). Increasing summer net CO₂ uptake in high northern ecosystems inferred from atmospheric inversions and comparisons to remote-sensing NDVI. *Atmospheric Chemistry and Physics*, 16(14), 9047–9066.
- Xia, J., Niu, S., Ciais, P., Janssens, I. A., Chen, J., Ammann, C., ... Luo, Y. (2015). Joint control of terrestrial gross primary productivity by plant phenology and physiology. *Proceedings of the National Academy of Sciences of the United States of America*, 112(9), 2788–2793. <https://doi.org/10.1073/pnas.1413090112>
- Xu, L., Myneni, R. B., Chapin III, F. S., Callaghan, T. V., Pinzon, J. E., Tucker, C. J., ... Stroeve, J. C. (2013). Temperature and vegetation seasonality diminishment over northern lands. *Nature Climate Change*, 3(6), 581–586. <https://doi.org/10.1038/nclimate1836>
- Yamori, W., Hikosaka, K., & Way, D. A. (2014). Temperature response of photosynthesis in C3, C4, and CAM plants: Temperature acclimation and temperature adaptation. *Photosynthesis Research*, 119(1–2), 101–117. <https://doi.org/10.1007/s11120-013-9874-6>
- Zhang, Y., Guanter, L., Berry, J. A., Joiner, J., van der Tol, C., Huete, A., ... Köhler, P. (2014). Estimation of vegetation photosynthetic capacity from space-based measurements of chlorophyll fluorescence for terrestrial biosphere models. *Global Change Biology*, 20(12), 3727–3742. <https://doi.org/10.1111/gcb.12664>
- Zhao, F., & Zeng, N. (2014). Continued increase in atmospheric CO₂ seasonal amplitude in the 21st century projected by the CMIP5 Earth system models. *Earth System Dynamics*, 5(2), 423.
- Zhao, M., Heinsch, F. A., Nemani, R. R., & Running, S. W. (2005). Improvements of the MODIS terrestrial gross and net primary production global data set. *Remote Sensing of Environment*, 95(2), 164–176. <https://doi.org/10.1016/j.rse.2004.12.011>
- Zhou, S., Zhang, Y., Ciais, P., Xiao, X., Luo, Y., Caylor, K. K., ... Wang, G. (2017). Dominant role of plant physiology in trend and variability of gross primary productivity in North America. *Scientific Reports*, 7, 41366. <https://doi.org/10.1038/srep41366>

SUPPORTING INFORMATION

Additional supporting information may be found online in the Supporting Information section at the end of the article.

How to cite this article: Park T, Chen C, Macias-Fauria M, et al. Changes in timing of seasonal peak photosynthetic activity in northern ecosystems. *Glob Change Biol*. 2019;00:1–14. <https://doi.org/10.1111/gcb.14638>